27 Jul 2022

High-Performance Catalytic Four-Channel Hollow Fibers with Highly Dispersed Nickel Nanoparticles Prepared by Atomic Layer Deposition for Dry Reforming of Methane

Baitang Jin

Shiguang Li

Xinhua Liang
Missouri University of Science and Technology, liangxin@mst.edu

Recommended Citation

B. Jin et al., "High-Performance Catalytic Four-Channel Hollow Fibers with Highly Dispersed Nickel Nanoparticles Prepared by Atomic Layer Deposition for Dry Reforming of Methane," *Industrial and Engineering Chemistry Research*, vol. 61, no. 29, pp. 10377 - 10386, American Chemical Society, Jul 2022. The definitive version is available at https://doi.org/10.1021/acs.iecr.1c03705

I&EC research
Industrial & Engineering Chemistry Research
pubs.acs.org/IECR
Article

High-Performance Catalytic Four-Channel Hollow Fibers with Highly Dispersed Nickel Nanoparticles Prepared by Atomic Layer Deposition for Dry Reforming of Methane

Baitang Jin, Shiguang Li, and Xinhua Liang*

Cite This: *Ind. Eng. Chem. Res.* 2022, 61, 10377−10386
Read Online

ABSTRACT: Highly dispersed nickel (Ni) nanoparticles (NPs) with an average particle size of 4.3 nm were uniformly deposited on the outer surface, the inner channel surface, and inside the pores of 20 cm long four-channel α-Al_2O_3 hollow fibers (HFs) by atomic layer deposition (ALD) for dry reforming of methane (DRM). Cerium oxide (CeO_2) was added to promote the catalytic performance of Ni/Al_2O_3−HF catalysts. Rationally designed filling methods, by tuning the reactor size and inert fillings, can reduce the catalyst bed voidage in a fixed bed reactor for better reactant gas distribution, effectively utilize the Ni reactive sites, and achieve excellent catalytic performance. It was found that the CeO_2-promoted Ni/Al_2O_3−HF catalyst was highly active and highly stable without deactivation during an overall 400-h DRM test at 850 °C. CeO_2 with reversible valence states could participate in surface reactions; especially, the formation of $CeAlO_3$ provided sufficient surface Ce^{3+} for CO_2 activation and enhanced the stability and reusability of the HF catalysts.

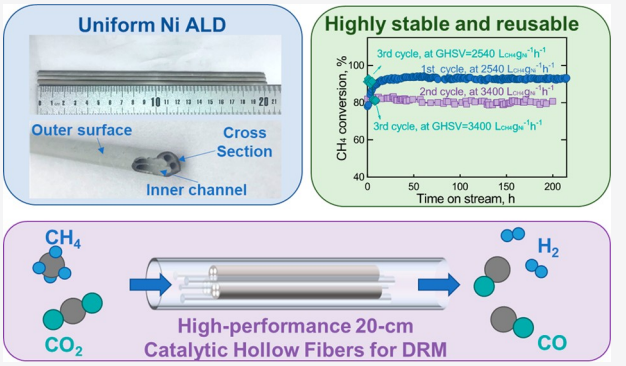

1. INTRODUCTION

With the increasing demand in dealing with CO_2 emission from fossil fuels, industry-scale carbon fixation technology via CO_2 utilization is highly demanded.[1−4] Dry reforming of methane (DRM) has drawn a great deal of interest from researchers by offering an economically feasible route to deal with the excessive CO_2 emission and converting two greenhouse gases into valuable synthesis gas (syngas).[1,5] Besides, DRM could effectively utilize the main components (CH_4 and CO_2) of biogas from the digestion of biomass and incorporate them into the renewable energy system.[6−8] Although DRM has not been applied for industrial applications, DRM exhibits great potential in lowering the CO_2 footprint for decarbonization milestones and producing syngas with a low H_2/CO ratio suitable for C_{5+} production.[9−13] Nickel-based catalysts, with low cost and high initial activity, are intensively investigated for DRM,[9] and the catalytic performance can be further improved by introducing promoters, such as CeO_2,[14,15] MgO,[16,17] and La_2O_3.[18]

For potential industrial application of DRM, a pressure drop in the catalyst bed is directly related to the operating cost and safety of the fixed bed reformer, and thus, the support shape is a very critical factor for DRM catalyst design.[9,19] The geometric property of multichannel design can allow a much higher throughput rate without causing a corresponding high pressure drop and equipment impairment.[9] Mathematical modeling demonstrated that the multichannel cylinder-shaped catalyst support could achieve high effectiveness, low pressure drop, and excellent heat transfer performance, as compared to sphere-shaped, cylinder-shaped, or single-channel cylinder-shaped catalysts.[20] Besides, it was reported that a four-channel cylinder-shaped catalyst had the highest methane conversion in the practical DRM test among different shaped catalysts (e.g., sphere, cylinder, trilobe, Raschig ring, and four-channel cylinder).[21] Due to its high thermal and mechanical stability and strong interaction with Ni nanoparticles,[22,23] Al_2O_3 is commonly used as a support for Ni-based catalysts for the DRM reaction. In this study, a 20 cm long four-channel structured α-Al_2O_3 hollow fiber (HF) was chosen as the catalyst support for the DRM reaction, with a high surface area to volume ratio (3,000 m^2 m^{-3}), which is much higher than that of regular catalyst supports,[24] and a low-pressure drop due to its channeling design.[25]

Ultrasmall Ni nanoparticles (NPs) can provide high catalytic activity for DRM and limit the graphitic carbon growth by size limitation.[1,26] Compared to relatively large Ni NPs prepared by

Special Issue: Engineered Methodologies for CO2 Utilization

Received: September 13, 2021
Revised: November 4, 2021
Accepted: November 30, 2021
Published: December 14, 2021

traditional liquid methods, atomic layer deposition (ALD) can deposit small Ni NPs uniformly on the Al_2O_3 substrate. Besides nm-scale or μm-scale catalyst substrates (e.g., nanoparticles or micron-size particles), only a few works have contributed to extending ALD to mm-level scale or cm-level scale porous substrates, such as flat membranes or HFs.[27−29] Especially, for mm- or cm-scale 3D geometric structures, it would be highly desired to uniformly deposit film or NPs with Ångström level precision on the 3D-structure substrate.[30] As for a tubular structure, TiO_2 ALD thin film was uniformly coated on 10 cm long polysulfone HFs in a forced-flow ALD reactor,[27] and Al_2O_3 ALD thin film was coated on porous polypropylene hollow fibers for better membrane performance.[29] However, ALD has not been applied to deposit active metal NPs onto large complex substrates, such as ceramic HFs with an ∼20 cm length in this study. It would be important to utilize ALD technology to deposit metal NPs onto large substrates.

In this work, Ni NPs were uniformly deposited on 20 cm long HFs by ALD, followed by the addition of CeO_2 as a promoter using the traditional incipient wetness method to prepare high-performance HF-supported Ni-based catalysts. Multiple 20 cm long hollow fibers were tested for DRM reactions with high gas flow rates. Long-term stability tests of a total of ∼400 h at 850 °C were conducted, and the regeneration process for catalyst recycling was studied in detail.

2. EXPERIMENTAL SECTION

2.1. Catalyst Preparation. Four-channel α-Al_2O_3 HFs,[25] as shown in Figure 1a, were used as catalyst supports. The HFs had a diameter of ∼3.36 mm and a length of 20 cm, with a channel diameter of ∼0.97 mm. ALD was used to deposit Ni NPs on 20 cm long four-channel α-Al_2O_3 HFs by a homemade ALD reactor, as schematically shown in Figure 1b (details described in our previous work).[31] Bis(cyclopentadienyl)nickel ($NiCp_2$, Alfa Aesar) and hydrogen (Airgas, 99.99%) were used as precursors for Ni ALD, and the reaction temperature was set at 300 °C. Several 20 cm long HFs were loaded in the reactor, as shown in Figure 1b. Before ALD, the HFs in the reactor were preheated at 150 °C overnight to remove any moisture adsorbed on HFs. During the first half cycle of Ni ALD, $NiCp_2$ vapor was delivered into the reactor from a bubbler heated at 85 °C using N_2 as a carrier gas; the dosing time was 600 s for sufficient chemisorption of $NiCp_2$ on the HFs, unless it was specifically mentioned. Then, the hollow fibers underwent a flush in 6 mL min^{-1} N_2 for 600 s, followed by an evacuation process by a vacuum pump for 10 s. In the second half-reaction of Ni ALD, procedures with the same period were conducted but using H_2 as a precursor to remove the organic ligands left on Ni precursors adsorbed on the substrate surface. In this study, two cycles of Ni ALD were conducted, and the samples were denoted as Ni/Al_2O_3−HF catalysts. The Ni loading was 0.091 ± 0.005 wt %.

The incipient wetness (IW) method was used to introduce CeO_2 onto the Ni/Al_2O_3−HF catalyst. $Ce(NO_3)_3{\cdot}6H_2O$ (cerium nitrate hexahydrate, Alfa Aesar, 99.99%) was used as the precursor. The Ni/Al_2O_3−HF catalyst was soaked in a $Ce(NO_3)_3$ solution for 1 h, dried at 100 °C under continuous stirring, and then calcined in air at 500 °C for 3 h. The samples were denoted as CeO_2−Ni/Al_2O_3−HF catalysts. The Ce loading was 0.010 wt %.

For X-ray photoelectron spectroscopy (XPS) and hydrogen temperatue-programed reduction (H_2-TPR) analysis, α-Al_2O_3 nanoparticles were used as catalyst supports. Ni NPs were deposited by ALD, and CeO_2 was added as the promoter by the IW method, using the same procedures for HF catalysts.

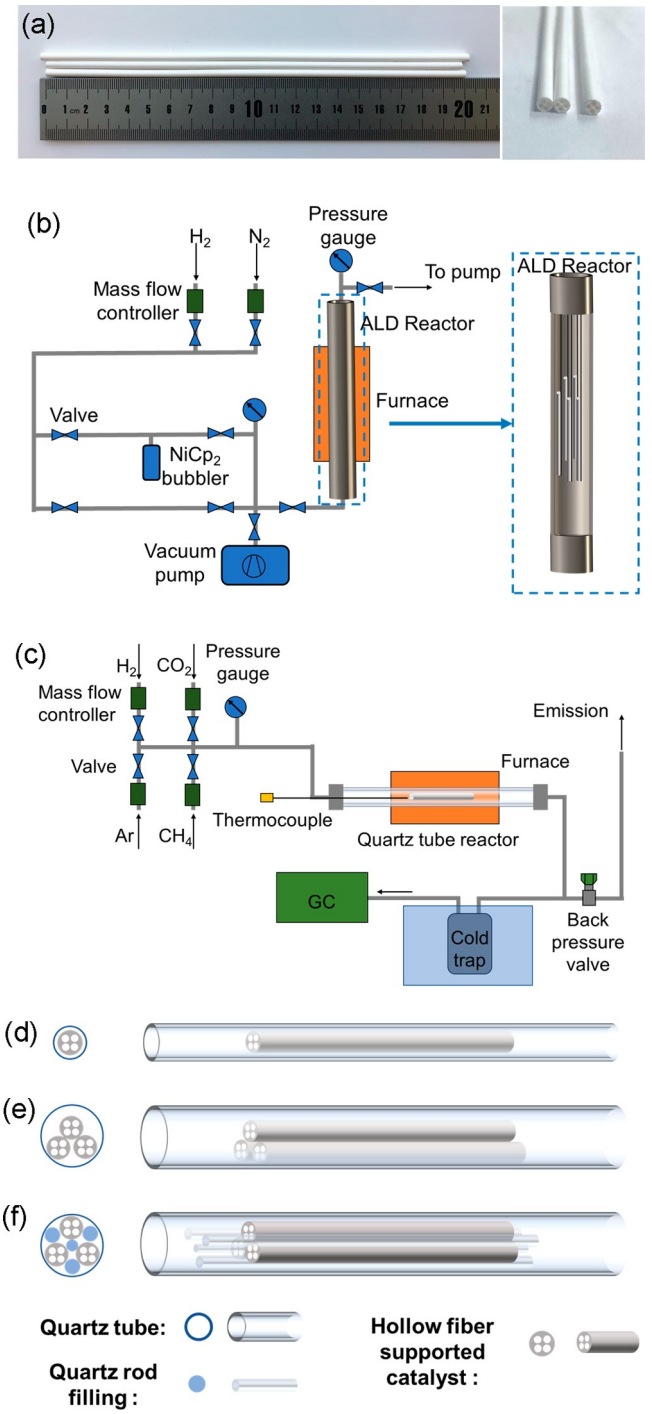

Figure 1. (a) Photo of four-channel α-Al_2O_3 hollow fibers and schematic images of (b) the ALD reactor system for Ni ALD on multiple 20 cm hollow fibers with the scheme of HFs loaded in the ALD reactor and (c) the DRM reactor system and (d, e, f) different catalyst loading methods for HF supported catalysts: (d) a single HF catalyst in the 4 mm i.d. quartz tube reactor, (e) three HF catalysts in the 8 mm i.d. quartz reactor without quartz rod fillings, and (f) three HF catalysts in the 8 mm i.d. quartz tube reactor with quartz rod fillings.

2.2. Dry Reforming of Methane Reaction. The dry reforming of methane reaction was carried out in a homemade

https://doi.org/10.1021/acs.iecr.1c03705
Ind. Eng. Chem. Res. 2022, 61, 10377−10386

fixed bed catalytic reactor system, as shown schematically in Figure 1c. One tube furnace (Carbolite Gero, Ltd.) was used for heat supply. Mass flow controllers (MKS Instruments) were used to control the gas flow rates. K-type thermocouples (Omega Engineering) were used to measure the temperature inside the quartz tube reactor. A gas chromatograph (SRI 8610C) was used to analyze the compositions of the gas product. A cold trap tank was set to remove any water generated as the byproduct. The reactor pressure was monitored by a pressure gauge and kept constant at atmospheric pressure.

Different catalyst bed filling methods were tested for HF-supported catalysts in DRM reactions, as shown in Figures 1d−1f. A quartz tube with 4 mm i.d. was used to fit a single HF catalyst, as shown in Figure 1d. To accommodate more HFs for scale-up purpose, a quartz tube with 8 mm i.d. was used for three 20 cm HFs, as shown in Figure 1e. Besides, several inert quartz rods were used as fillings for better gas distribution for three 20 cm HF tests in an 8 mm i.d. quartz tube, as shown in Figure 1f.

Before the reaction, the catalyst sample was first reduced in 100 mL min^{-1} 20 vol % H_2/80 vol % Ar at 800 °C for 1 h. The temperature ramped to 850 °C at 10 °C min^{-1} in Ar flow, and then, Ar gas was switched to the reactant gas (50 vol % CH_4/50 vol % CO_2) when the temperature reached 850 °C. In this study, the DRM reaction for a certain time without returning to ambient temperature and without regeneration to remove coking was defined as a cycle of DRM reaction. To test the recyclability of the Ni/Al_2O_3−HF catalysts, a regeneration process between cycles of the DRM test consisted of oxidation in 100 mL min^{-1} 20 vol % O_2/80 vol % Ar gas flow at 700 °C for 1 h first and then reduction at 800 °C in 100 mL min^{-1} 20 vol % H_2/80 vol % Ar gas flow for 1 h.

2.3. Catalyst Characterization. Inductively coupled plasma-optical emission spectroscopy (ICP-OES) was applied to analyze the Ni content on the HF catalyst, using 2000D PerkinElmer. H_2SO_4, H_3PO_4, and H_2O_2 were used to digest the HF-supported catalysts for ICP-OES. Transmission electron microscopy (TEM) was applied to measure the size of the deposited Ni NPs using an FEI Tecnai F20 transmission electron microscope. XPS was conducted using a Kratos Axis 165 X-ray photoelectron spectrometer, using monochromatic Al Kα as the radiation source. X-ray diffraction (XRD) was conducted using a Philips X-Pert multipurpose diffractometer. H_2-TPR was conducted using a Micromeritics AutoChem II 2920 with 10 vol % H_2/90 vol % Ar admix gas from 100 to 900 °C at 10 °C/min. Temperature-programmed oxidation (O_2-TPO) was conducted using the homemade reactor with a QMS200 mass spectrometer (Stanford Research System) in a 10 vol % O_2/90 vol % Ar gas mixture from 100 to 900 °C at 10 °C/min.

3. RESULTS AND DISCUSSION

3.1. Deposition of Ni NPs on a 20 cm Long HF by ALD. In our previous study, HFs were broken into short pieces (~0.8 cm long) and then deposited by Ni ALD.[31] To achieve scale-up production of the ALD-prepared 20 cm long Ni/Al_2O_3−HF, multiple 20 cm HFs were directly hung in the reactor for Ni ALD, and the dosing time was investigated as an important factor. Figure 2 depicts the effects of the dosing time on Ni loading and catalytic performance of the catalysts for the DRM test. In Figure 2a, for the 20 cm long Al_2O_3−HF support, the Ni loading increased when the dosing time

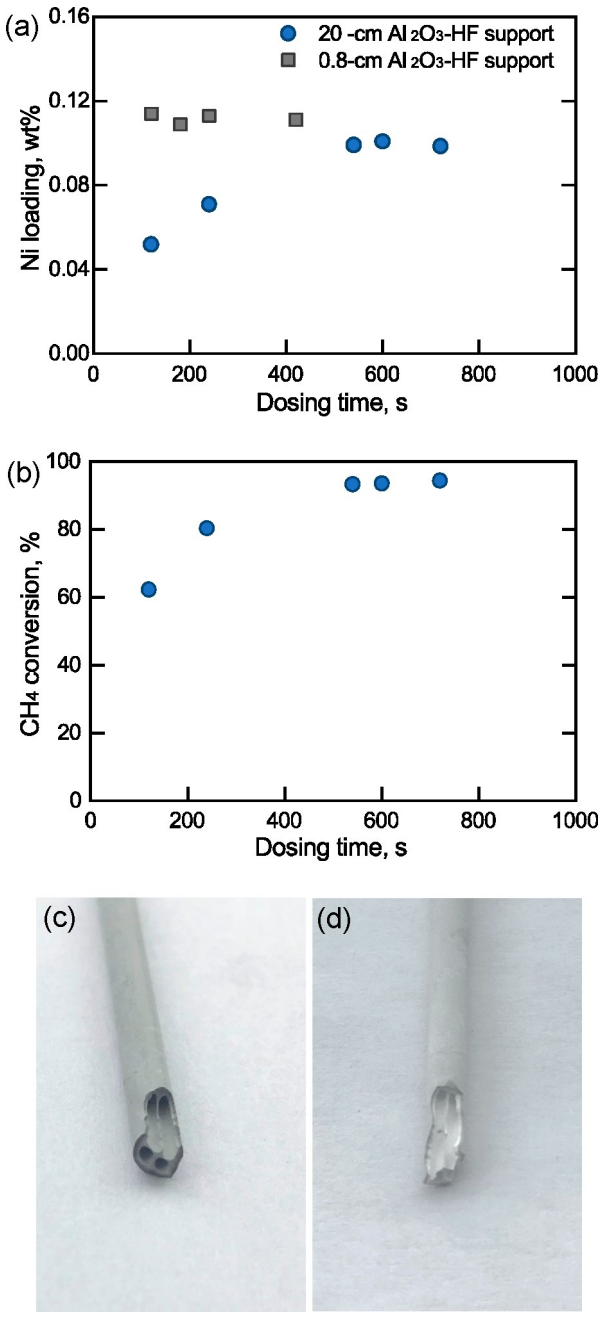

Figure 2. Effects of the precursor dosing time during Ni ALD on (a) Ni loading of the 20 cm long Ni/Al_2O_3−HF catalyst and (b) CH_4 conversion for the DRM test. Four-cm middle parts from the 20 cm long Ni/Al_2O_3−HF catalyst prepared by ALD were used as catalysts for the DRM reaction. Photos of the cross-sectional surface of the HF cut from the middle part of the 20 cm long Ni/Al_2O_3−HF with Ni ALD dosing times of (c) 600 s and (d) 120 s.

increased from 120 to 240 s, and the Ni loading reached a constant value when the dosing time further increased from 560 to 720 s. The increase of Ni loading with the increase of the dosing time indicated that the substrate surface was not saturated with the Ni precursor, so $NiCp_2$ continued to react with surface hydroxyl groups until the chemisorption of $NiCP_2$ on the Al_2O_3−HF surface was saturated.[32,33] Besides, the catalytic performance of the catalysts exhibited a similar tendency as the Ni loading increased, as shown in Figure 2b and Figure S1. Notably, there is no such trend for Ni loading

https://doi.org/10.1021/acs.iecr.1c03705
Ind. Eng. Chem. Res. 2022, 61, 10377−10386

on the 0.8 cm Al_2O_3−HF vs the ALD precursor dosing time. Very similar Ni loading values were found for Ni ALD on the 0.8 cm Al_2O_3−HF as the precursor dosing time increased, indicating that the saturation of $NiCp_2$ on the 0.8 cm Al_2O_3−HF was much quicker than that on the 20 cm long Al_2O_3−HF even with a shorter precursor dosing time. For Ni ALD scaling-up from the 0.8 to 20 cm Al_2O_3−HF support, the longer hollow fibers required a longer precursor dosing time to reach the saturation state for the chemisorption because of the longer diffusion length in the long HFs; a longer saturation time could be needed for the upper part of the 20 cm Al_2O_3−HF because the $NiCp_2$ precursor entered the ALD reactor from the bottom. Ascribed to the self-limiting nature of ALD, the chemisorption of $NiCP_2$ could be saturated once the surface sites were occupied when the dosing time was sufficient, and thus the geometric difference would not lead to partial accumulation, resulting in a uniform and repeatable deposition of Ni NPs.

Figures 2c and 2d exhibit the morphology of the HF catalysts that were cut from the 20 cm long Ni/Al_2O_3−HF catalysts. For the 20 cm Ni/Al_2O_3−HF with a dosing time of 120 s, the inner channel was almost white (the same color as the Al_2O_3 HF support), while the outer surface was gray, indicating that the low dosing time was not enough for the precursor to diffuse into the inner channel, especially for the 20 cm long HFs. In contrast, for the 20 cm Ni/Al_2O_3−HF with a dosing time of 600 s, both the HF surface and the inner channel surface are gray, which resulted from the full saturation of both outer and inner surfaces with a long precursor dosing time. Besides, the cross-section of the 20 cm Ni/Al_2O_3−HF with a dosing time of 600 s was also gray, the same as that of the inner channel and outer surface. During the ALD process, the precursor molecules could not only enter the inner channel from both ends of the hollow fibers but also diffuse into the inner channel from the outer surface via the pore of hollow fibers (~0.9 μm[25]). These Ni NPs in the pores would be accessible for the reactant gases during DRM.

Different techniques were used to verify the uniformity of Ni NPs deposited on HF substrates. As shown in Figure 3, the ALD-prepared 20 cm Ni/Al_2O_3−HF was uniformly gray, as compared to the white fresh HFs (Figure 1a), indicating the uniform deposition of Ni NPs by ALD. The Ni/Al_2O_3−HF catalysts were also checked by TEM, as shown in Figure 3b. The average size of Ni NPs was about 4.3 nm, with high and uniform Ni dispersion. In addition, ICP-OES results in Figure 3c indicate that the Ni loadings on different HFs were similar for the same batch of ALD-prepared 20 cm long Ni/Al_2O_3−HFs.

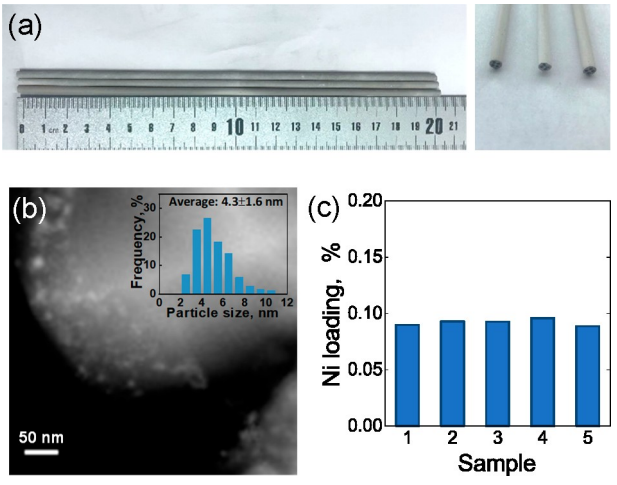

Figure 3. (a) Photos of the 20 cm long Ni/Al_2O_3−HF after 2 cycles of Ni ALD and (b) the STEM image of the ALD-prepared Ni/Al_2O_3−HF. (c) Ni ICP-OES results of ALD-prepared Ni/Al_2O_3−HF catalysts from one batch of Ni ALD.

To indirectly check whether Ni NPs were uniformly deposited on 20 cm long HFs, one 20 cm long Ni/Al_2O_3−HF was broken into three pieces, i.e., upper part, middle part, and lower part. Each piece was about 4 cm long and was tested for the DRM reaction. The DRM results are shown in Figure 4.

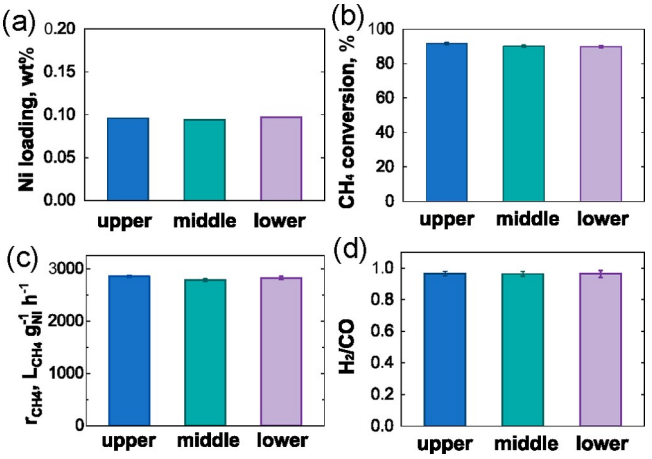

Figure 4. (a) Ni loading, (b) CH_4 conversion, (c) CH_4 reforming rate, and (d) H_2/CO ratio using a 4 cm upper part, a 4 cm middle part, and a 4 cm lower part (cut from a 20 cm long Ni/Al_2O_3−HF prepared by ALD) for the DRM test in a quartz tube reactor with 4 mm i.d.

Each piece from different parts of one single 20 cm long HF exhibited similar methane conversion, methane reforming rates, and H_2/CO ratio for the DRM test, which confirmed that the ALD process could uniformly deposit Ni NPs on multiple 20 cm long hollow fibers. In this study, the 20 cm long HFs were hung vertically in a vertical ALD tube reactor, and the precursors were fed from the bottom of the reactor; the saturation of precursor adsorption on the HFs' surface could be achieved so that the effects of position difference of HFs were not that significant, which was ascribed to the self-limitation and self-termination nature of the ALD process. In one word, ALD could be upscaled to prepare multiple 20 cm long HF catalysts with excellent uniformity and high dispersion of Ni NPs.

3.2. Effects of the Filling Method of HF-Supported Catalysts. The filling method of the catalyst bed could be an important factor for the DRM test. As shown in Figure 5 and Figure S2, three types of bed filling methods for HF catalysts in a quartz tube reactor were studied. Notably, the different filling methods of HF-supported Ni catalysts resulted in different catalytic performances, and the addition of CeO_2 as the promoter significantly improved the activity for the Ni/Al_2O_3−HF catalyst, which will be discussed in the next section. For the filling method, it could be seen that the best performance was achieved by loading a single Ni/Al_2O_3−HF or CeO_2−Ni/Al_2O_3−HF in a 4 mm i.d. quartz tube with a minimum void between the reactor and HF, with ~95% CH_4 conversion at

https://doi.org/10.1021/acs.iecr.1c03705
Ind. Eng. Chem. Res. 2022, 61, 10377−10386

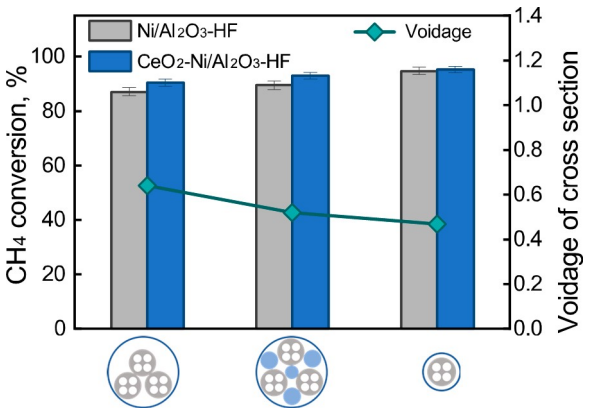

Figure 5. CH_4 conversion and voidage of the cross-section area of the catalyst bed for different catalyst bed filling methods of 20 cm Ni/Al_2O_3−HFs and 20 cm CeO_2−Ni/Al_2O_3−HFs for DRM at 850 °C at GHSV of 2,850 ± 50 L_{CH_4} g_{Ni}^{-1} h^{-1}.

gas hourly space velocity (GHSV) of about 2,850 L_{CH_4} g_{Ni}^{-1} h^{-1}, whereas three packed 20 cm CeO_2−Ni/Al_2O_3−HFs showed a comparable conversion of ∼93% in an 8 mm i.d. quartz tube with inert quartz rod fillings between HFs. For three 20 cm CeO_2−Ni/Al_2O_3−HFs, the conversion was ∼89% without any inert fillings, as compared to ∼93% of the case with inert fillings.

The voidage of the catalyst bed, which is defined as the proportion of the unoccupied volume in a catalyst bed,[21] is considered an important factor for the filling method. Take the Ni/Al_2O_3−HF as an example, the least bed voidage at 0.47 and the highest methane conversion at 94.6% were achieved for a single HF in a 4 mm i.d. quartz tube. Using the same three 20 cm Ni/Al_2O_3−HFs inside an 8 mm i.d. quartz tube reactor, a voidage of 0.52 and a methane conversion of 89.5% were achieved with the usage of inert fillings, whereas a higher voidage of 0.64 and a lower methane conversion of 87% were achieved without any inert fillings. As discussed in the previous section, Ni NPs prepared by ALD were deposited everywhere on the porous HF support, including the outer surface, the inner surface, and inside the pores of the HFs. The inert quartz rod fillings can prevent gas "bypass" and distribute/drive the reactant gas into the inner channel and the pores of HFs. The irrational catalyst bed design might lead to an unbalanced reactant gas distribution, and some Ni sites surrounding more void areas might need to catalyze more reactant gas, whereas some Ni sites might only catalyze a few molecules of reactant gases and not be efficiently utilized. For instance, for the three 20 cm HFs without inert fillings, the Ni sites of one upper HF would catalyze more reactant gas, whereas the lower two would catalyze less reactant gases, similar to the "bypass". By rationally filling the catalyst bed, the voidage could be effectively reduced, therefore increasing the contact between gas and catalyst and increasing overall reactant conversion.

3.3. CeO_2-Promoted Ni/Al_2O_3−HF Catalysts. To prepare a high-performance Ni/Al_2O_3−HF catalyst, CeO_2 was used as a promoter to enhance the catalytic performance. One single 20 cm Ni/Al_2O_3−HF catalyst and one single 20 cm CeO_2−Ni/Al_2O_3−HF catalyst were tested at 850 °C for DRM in a 4 mm i.d. quartz tube. As shown in Figure 6, during 48 h of the DRM reaction, both the Ni/Al_2O_3−HF and CeO_2−Ni/Al_2O_3−HF exhibited methane conversion around ∼95% and a H_2/CO ratio around 0.97. Ni/Al_2O_3−HF exhibited a gradual

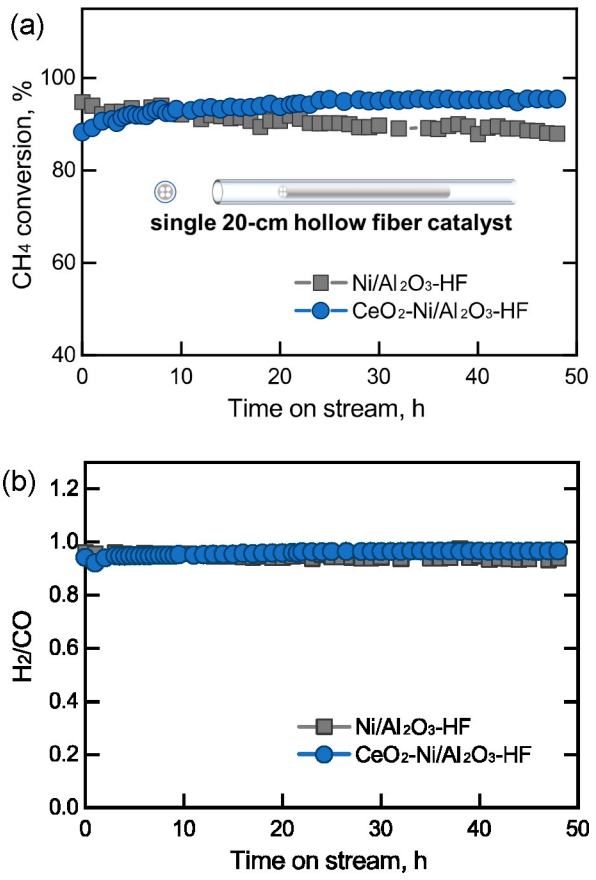

Figure 6. (a) CH_4 conversion and (b) H_2/CO ratio during the DRM reaction using a single 20 cm Ni/Al_2O_3−HF and a single 20 cm CeO_2−Ni/Al_2O_3−HF in a 4 mm i.d. quartz tube at 850 °C. GHSV = 2,850 L_{CH_4} g_{Ni}^{-1} h^{-1} with a total flow rate of 220 mL min^{-1}.

deactivation behavior, with methane conversion decreasing from 94.7% to 88.4% within 48 h of the reaction. In contrast, the CeO_2−Ni/Al_2O_3−HF had an activation behavior in the initial 20 h, from 88.4% to 95.3%, which could be ascribed to further reduction of Ni(II) to active Ni(0) sites due to the presence of CeO_2. Besides, the H_2/CO ratio also increased from 0.94 to 0.97 due to the activation behavior. As shown in Table 1, the activity of the CeO_2−Ni/Al_2O_3−HF in this work exhibited great activity, compared to some other high-performance catalysts from the literature. After 20 h of the DRM reaction, the methane conversion of the CeO_2−Ni/Al_2O_3−HF was highly stable, indicating that CeO_2 could significantly enhance the stability of the Ni/Al_2O_3−HF during DRM conditions, in terms of coke formation or sintering.

To get insight into the effects of CeO_2 for the enhancement of the catalytic performance, the Ni/Al_2O_3−HF and CeO_2−Ni/Al_2O_3−HF catalysts were tested under different values of GHSV, as shown in Figure 7 and Figure S3. At low GHSV (∼830 L_{CH_4} g_{Ni}^{-1} h^{-1}), the Ni/Al_2O_3−HF and CeO_2−Ni/Al_2O_3−HF exhibited identical conversion of ∼96% with the H_2/CO ratio at ∼0.97, which was close to the equilibrium conversion. At GHSV of ∼1,660 L_{CH_4} g_{Ni}^{-1} h^{-1}, the CH_4 conversion of the CeO_2−Ni/Al_2O_3−HF still reached the equilibrium conversion (∼96%) with the H_2/CO ratio at ∼0.97, whereas the conversion of the Ni/Al_2O_3−HF decreased to ∼92% with the H_2/CO ratio at 0.96, indicating a higher reaction rate of the CeO_2−Ni/Al_2O_3−HF. At a higher value of

https://doi.org/10.1021/acs.iecr.1c03705
Ind. Eng. Chem. Res. 2022, 61, 10377−10386

Table 1. Comparison of the Catalytic Performance for DRM in This Work and the Literature

		DRM catalytic performance				
catalyst	preparation method	GHSV, mL/g_{cat}/h	temp, °C	X_{CH_4}, %	r_{CH_4}, L_{CH_4}/g_{Ni}/h	ref
CeO_2−Ni/Al_2O_3−HF	**ALD**	**6,500**	**850**	**95**	**2,700**	**this work**
Ni/Al_2O_3	ALD	36,000	850	97	1,840	34
Ni/Al_2O_3−ZrO_2	impregnation+ plasma	60,000	850	94.5	285	35
Ni/ZSM-5	impregnation	12,000	800	95	114	36
Ni/$Ce_{0.2}Zr_{0.8}O_2$	coprecipitation	216,000	800	92	442	37
Ni−Mo/SBA-15-La_2O_3	impregnation	12,000	800	98	120	38
MgO-Ni/SBA-15	impregnation	36,000	800	97	175	39
Ni−Ce/Mg−Al-O	impregnation	72,000	800	93	280	40
Ni−Zr/MCM-41	coprecipitation	50,000	800	95	590	41
Ni−CaO−ZrO_2	coprecipitation	158,000	850	90	430	42

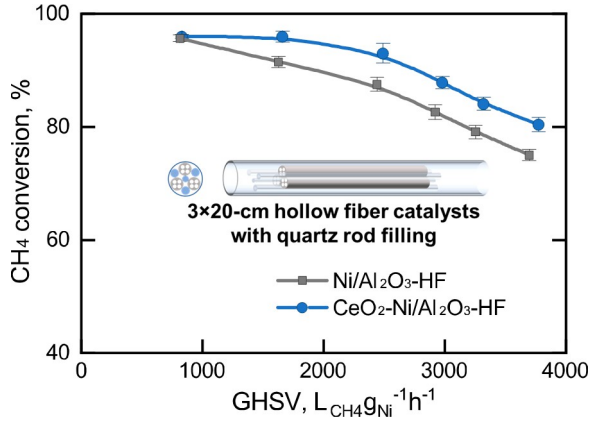

Figure 7. CH_4 conversion as a function of GHSV for DRM reactions using three HFs of a 20 cm long Ni/Al_2O_3−HF and three HFs of a 20 cm CeO_2−Ni/Al_2O_3−HF for DRM at 850 °C.

GHSV, the effect of equilibrium was less significant, and therefore, the CeO_2−Ni/Al_2O_3−HF exhibited higher activity than that of the Ni/Al_2O_3−HF. For instance, at GHSV of ∼2,980 L_{CH_4} g_{Ni}^{-1} h^{-1}, the CH_4 conversion of the CeO_2−Ni/Al_2O_3−HF reached ∼88% with the H_2/CO ratio at ∼0.94, as compared to the CH_4 conversion at ∼83% and the H_2/CO ratio at ∼0.92 of the Ni/Al_2O_3−HF. In short, CeO_2 could significantly improve the activity of the Ni/Al_2O_3−HF catalyst for DRM.

To study the effects of CeO_2 on the chemical states of the Ni element, Figure 8a illustrates the Ni 2p 3/2 XPS spectra of the reduced Ni/Al_2O_3 and reduced CeO_2−Ni/Al_2O_3 catalysts. All XPS spectra were calibrated at 284.5 eV using the adventitious carbon in C 1s (as shown in Figure S4). Ni could be deconvoluted into various species, with the metallic Ni peak located at ∼852.0 eV, NiO located at ∼854.4 eV, and $NiAl_2O_4$ located at ∼856.4 eV. Besides, due to the shakeup phenomena of the peaks, the satellite peaks of Ni(0) and Ni(II) were located at ∼857.9 eV and ∼861.3 eV, respectively.[43] Among the Ni species, the spinel $NiAl_2O_4$ was highly stable, even under highly reductive, high-temperature DRM reaction conditions, and the existence of $NiAl_2O_4$ indicated that the interaction between NiO and Al_2O_3 in the ALD-prepared Ni/Al_2O_3 catalyst was too strong to be completely reduced to active metallic Ni sites.[22,44] Compared to the reduced Ni/Al_2O_3 catalyst, the reduced CeO_2−Ni/Al_2O_3 catalyst exhibited a smaller amount of $NiAl_2O_4$ and more metallic Ni in the XPS spectra, which indicated that CeO_2 could improve the

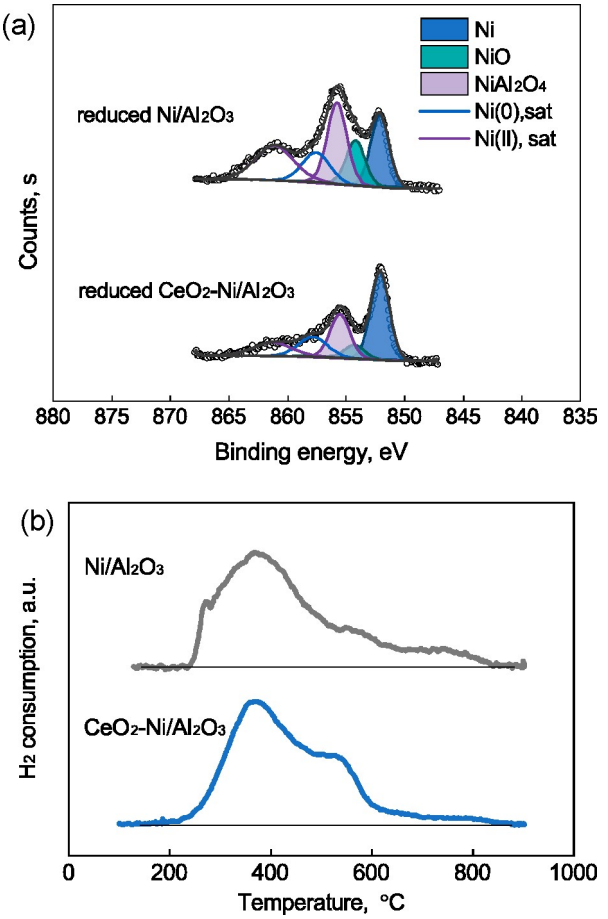

Figure 8. (a) XPS spectra of Ni 2p3/2 core levels of reduced Ni/Al_2O_3 and reduced CeO_2−Ni/Al_2O_3 and (b) the H_2-TPR profiles of the Ni/Al_2O_3 and CeO_2−Ni/Al_2O_3.

reducibility of $NiAl_2O_4$ and release more active metallic Ni sites from $NiAl_2O_4$.

H_2-TPR in Figure 8b was conducted to determine the interaction between Ni and the support. Generally, the peaks for the Ni/Al_2O_3 system could be assigned to NiO (free from Al_2O_3) at ∼400 °C, NiO-Al_2O_3 (NiO interacted with Al_2O_3) at 500−700 °C, and spinel $NiAl_2O_4$ at 800 °C, respectively.[22,45] In our previous work, the interaction between NiO and Al_2O_3 for the Ni/Al_2O_3 catalyst prepared by ALD was observed due to its unique chemisorption-based growth.[34] As shown in Figure 8b, it would be seen the H_2-TPR profile in the Ni/Al_2O_3 ranged from 240 to 850 °C, which indicated there were

https://doi.org/10.1021/acs.iecr.1c03705
Ind. Eng. Chem. Res. 2022, 61, 10377−10386

various species, including NiO, NiO-Al_2O_3, and $NiAl_2O_4$. For CeO_2−Ni/Al_2O_3, the H_2-TPR profile ranged from 210 to 830 °C, including NiO, NiO-Al_2O_3, and $NiAl_2O_4$. The lower reduction temperature indicated the CeO_2 enhanced the overall reducibility of the catalyst. Besides, it can be seen that there was less $NiAl_2O_4$ for CeO_2−Ni/Al_2O_4, meaning that CeO_2 could effectively assist the reduction of $NiAl_2O_4$ and keep Ni in a metallic state during DRM.

The morphology and lattice structure of the spent catalysts, i.e., Ni/Al_2O_3−HF and CeO_2−Ni/Al_2O_3−HF, were checked by STEM and XRD, as shown in Figure 9 and Figure S5. In

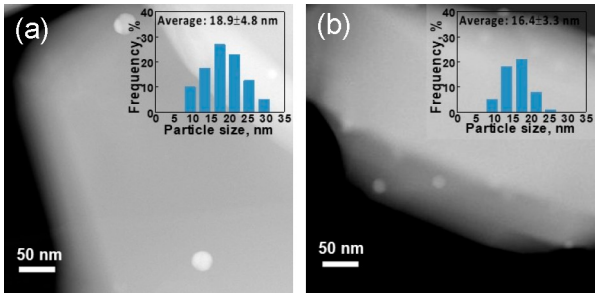

Figure 9. STEM images of the (a) spent Ni/Al_2O_3−HF and (b) spent CeO_2−Ni/Al_2O_3−HF catalysts.

TEM images, it could be seen that the spent Ni/Al_2O_3−HF catalyst had an average Ni particle size of 18.9 ± 4.8 nm, whereas the spent CeO_2−Ni/Al_2O_3−HF catalyst had an average Ni particle size of 16.4 ± 3.3 nm. The smaller average Ni particle size of the spent CeO_2−Ni/Al_2O_3−HF indicated that CeO_2 could also effectively inhibit the sintering of Ni NPs and enhance the stability of the catalyst during DRM reaction.

3.4. Long-Term Stability and Regeneration Tests. To scale up the DRM test with multiple HFs, three pieces of 20 cm long CeO_2−Ni/Al_2O_3−HF catalysts were tested in terms of stability and recyclability. Quartz rod fillers were applied to minimize the voids between CeO_2−Ni/Al_2O_3−HF catalysts. The results are shown in Figure 10. In this test, the total flow rate reached 660 mL min^{-1}, at GHSV of 2,540 L_{CH_4} g_{Ni}^{-1} h^{-1}. For the first cycle of DRM, the reactant gases were 660 mL min^{-1} (50 vol % CH_4/50 vol % CO_2). There was an obvious activation process in the initial 15 h of reaction, since the CH_4 conversion increased from 78% to 93% gradually. During the following 200 h of the test, notably, no deactivation was observed, indicating that the CeO_2−Ni/Al_2O_3−HF catalyst was highly stable for the DRM reaction.

To further investigate the stability and the recyclability of the catalyst, the CeO_2−Ni/Al_2O_3−HF catalyst underwent a regeneration process (first oxidized in 100 mL min^{-1} 20 vol % O_2/80 vol % Ar gas flow at 700 °C for 1 h and then reduced at 800 °C in 100 mL min^{-1} 20 vol % H_2/80 vol % Ar gas flow for 1 h), and then, it was tested under an even higher gas flow rate of 880 mL min^{-1}, at GHSV of 3,400 L_{CH_4} g_{Ni}^{-1} h^{-1}. Due to the much higher flow rate of feed gases, a lower CH_4 conversion of ∼81% was observed; there was no catalytic activity loss during this 400-h test including 200 h before regeneration and 200 h after regeneration. The same catalyst underwent another regeneration process, and then, it was tested for the third cycle of DRM at 2,540 L_{CH_4} g_{Ni}^{-1} h^{-1} and 3,400 L_{CH_4} g_{Ni}^{-1} h^{-1} to test the catalyst recyclability. The same CH_4 conversion and the same product composition (H_2/CO ratio of ∼0.96 at 2,540

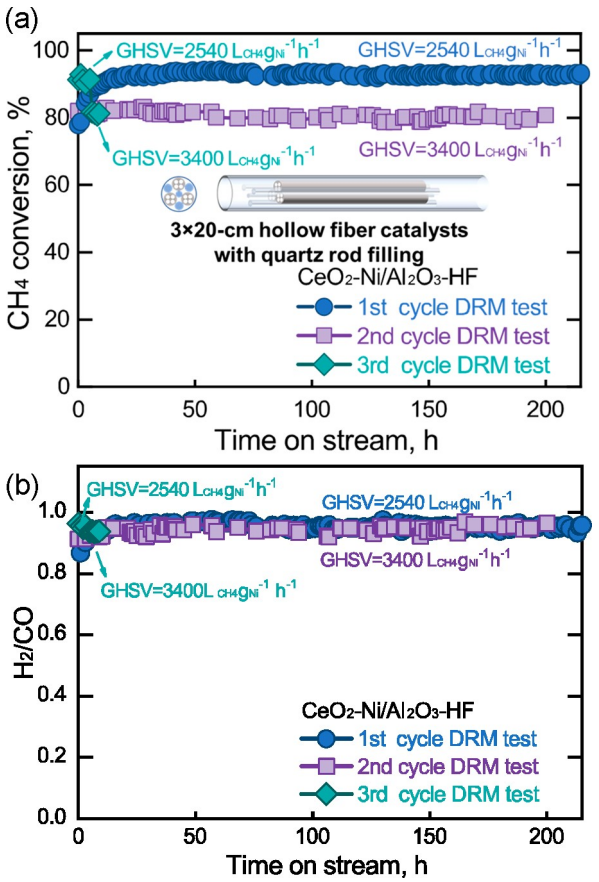

Figure 10. (a) CH_4 conversion and (b) H_2/CO ratio of the CeO_2−Ni/Al_2O_3−HF catalyst in gas flow for the long-term stability DRM test at 850 °C: the first cycle of DRM reaction at GHSV of 2,540 L_{CH_4} g_{Ni}^{-1} h^{-1}, the second cycle at GHSV of 3,400 L_{CH_4} g_{Ni}^{-1} h^{-1}, and the third cycle of DRM reaction at GHSV of 2,540 L_{CH_4} g_{Ni}^{-1} h^{-1} or 3,400 L_{CH_4} g_{Ni}^{-1} h^{-1}.

L_{CH_4} g_{Ni}^{-1} h^{-1} and ∼0.94 at 3,400 L_{CH_4} g_{Ni}^{-1} h^{-1}) were obtained, as compared to the results of the first cycle and second cycle of the DRM tests. Therefore, the CeO_2-promoted catalyst exhibited superior stability and recyclability for the DRM tests.

CeO_2 greatly enhanced the stability of the pristine Ni/Al_2O_3−HF catalyst and the regenerated catalyst for DRM, and no activity loss was found for the regenerated CeO_2−Ni/Al_2O_3−HF. To get insight into catalyst regeneration, XPS was applied using the CeO_2−Ni/Al_2O_3 catalyst at different states, including reduced (the fresh catalyst underwent H_2-treatment), spent (the reduced catalyst further underwent DRM), oxidized (the spent catalyst further underwent oxidation), and regenerated (the oxidized catalyst further underwent H_2-treatment). For Ce 3d profiles in Figure 11a, Ce^{4+} includes Ce 3d5/2 peaks (v at 881.9 eV, v'' at 886.2 eV, and v''' at 897.8 eV) and Ce 3d3/2 peaks (u at 900.5 eV, u'' at 904.8 eV, and u''' at 916.3 eV), whereas Ce^{3+} includes Ce 3d5/2 peaks (v_o at 880.8 eV and v' at 884.6 eV) and Ce 3d3/2 peaks (u_o at 899.1 eV and u' at 903.1 eV).[46,47] Notably, the Ce element exhibited changeable chemical states, indicating that CeO_2 was not inert in the redox atmosphere and might participate in surface reactions.[47,48] The reversible oxidation state of Ce can achieve oxygen storage capacity and assist the oxygen transfer for catalytic reactions; therefore, the chemical state of Ce plays an

https://doi.org/10.1021/acs.iecr.1c03705
Ind. Eng. Chem. Res. 2022, 61, 10377−10386

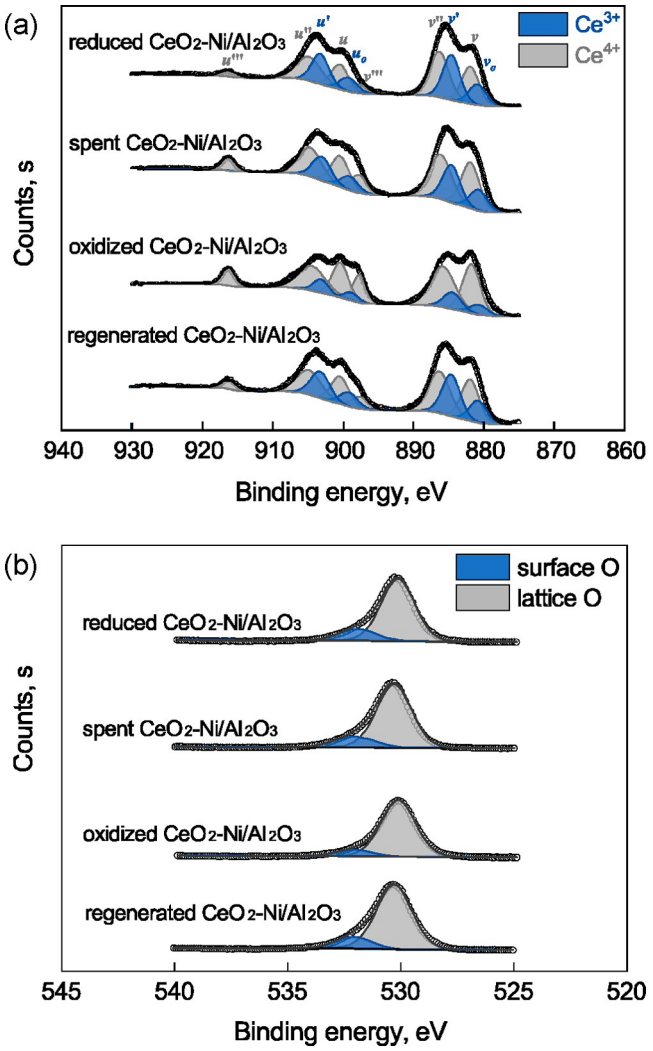

Figure 11. XPS spectra of (a) Ce 3d and (b) O 1s core levels of reduced CeO_2−Ni/Al_2O_3, spent CeO_2−Ni/Al_2O_3, oxidized CeO_2−Ni/Al_2O_3, and regenerated CeO_2−Ni/Al_2O_3.

important role in the catalytic reaction. Especially, CeO_x can interact with Al_2O_3 under a reductive atmosphere at high temperature (T > 500 °C), when Al^{3+} ions diffuse into the vacant sites of the CeO_x lattice at the CeO_x-Al_2O_3 interface, and $CeAlO_3$ will be favorably formed,[45,48,49] providing more Ce^{3+} than CeO_2 does.[45,48,49] For this work, a high concentration of Ce^{3+} was observed for the reduced or regenerated CeO_2−Ni/Al_2O_3 with a high Ce^{3+} ratio (v_o% + v'% + u_o% + u'%) at ∼39% and a low Ce^{4+} diagnostic peak (u'''%) at ∼3%, which were close to the reported values of $CeAlO_3$ but far from that of CeO_2 only.[50−52] Under this circumstance, the catalytic activity of the regenerated catalyst could be highly repeatable because of the reversible form of $CeAlO_3$ at the reductive atmosphere and CeO_2−Al_2O_3 mixed oxides at the oxidative atmosphere. In addition, the chemical states of oxygen species are shown in Figure 11b. It could be seen that the reduced and regenerated CeO_2−Ni/Al_2O_3 had more surface oxygen sites, which means that there were more coordinatively unsaturated oxygen sites or oxygen vacancy sites. The oxygen species under different chemical states also confirmed the variant roles of CeO_2 that participated in the catalytic surface reactions. During the DRM reaction, $CeAlO_3$ will act as CO_2 adsorption sites and participate in CO_2 dissociation, which helps store O-species originated from CO_2 and transfers O-species to the adsorbed CH_x for the DRM reaction. The enhanced CO_2 activation would benefit the DRM reaction and decrease the carbon formation, which was also demonstrated by O_2-TPO (Figure S6) that CeO_2 could strongly suppress the carbon formation.

4. CONCLUSIONS

In this work, Ni NPs were deposited on 20 cm long four-channel α-Al_2O_3 HFs by ALD for DRM. With a longer precursor dosing time during ALD than that for 0.8 cm long HFs, Ni NPs with an average particle size of 4.3 nm could be uniformly dispersed on the porous 20 cm long HF surfaces, including the inner channel surface, pores, and outer surface, whereas ALD with a short precursor dosing time could mainly deposit Ni NPs on the outer surface of HFs. The uniform deposition of Ni NPs was verified by TEM, ICP-OES, and catalytic testing of the catalysts from different parts of a single HF. Reducing the voidage of a catalyst bed, by adjusting the reactor tube size or adding inert fillings, can better distribute gas flow to achieve higher catalytic performance for DRM. It was found that a single HF catalyst in a 4 mm i.d. quartz tube reactor exhibited the best performance, and the three-packed 20 cm long CeO_2−Ni/Al_2O_3−HF showed comparable 93% conversion with inert quartz rods as filling in a quartz tube with an 8 mm i.d. A DRM test of three-packed 20 cm long CeO_2−Ni/Al_2O_3−HF catalysts exhibited excellent performance (93% conversion) at harsh conditions (850 °C, 660 mL min^{-1} 50 vol % CH_4/50 vol % CO_2 mixture), and no deactivation was observed for a 200-h DMR test followed by another 200-h test after catalyst regeneration. CeO_2 exhibited different valence states in the reductive/oxidative atmosphere. The formation of $CeAlO_3$ under H_2 atmosphere at the CeO_x-Al_2O_3 interface could stabilize Ce^{3+} and provide sufficient surface Ce^{3+}, which could serve as active sites for CO_2 activation and enhance the catalytic performance.

■ ASSOCIATED CONTENT

Supporting Information

The Supporting Information is available free of charge at https://pubs.acs.org/doi/10.1021/acs.iecr.1c03705.

H_2/CO ratio of activity test and stability test, XPS spectra of reduced and spent catalysts, XRD profiles of spent catalysts, and O_2-TPO profiles of spent catalysts (PDF)

■ AUTHOR INFORMATION

Corresponding Author

Xinhua Liang − *Linda and Bipin Doshi Department of Chemical and Biochemical Engineering, Missouri University of Science and Technology, Rolla, Missouri 65409, United States;* orcid.org/0000-0001-7979-0532; Email: Liangxin@mst.edu

Authors

Baitang Jin − *Linda and Bipin Doshi Department of Chemical and Biochemical Engineering, Missouri University of Science and Technology, Rolla, Missouri 65409, United States*

Shiguang Li − *Gas Technology Institute, Des Plaines, Illinois 60018, United States*

Complete contact information is available at: https://pubs.acs.org/10.1021/acs.iecr.1c03705

Notes

The authors declare no competing financial interest.

■ ACKNOWLEDGMENTS

This work was supported in part by the U.S. Department of Energy (Contract Number DE-FE0029760) and the Linda and Bipin Doshi Endowment of Missouri University of Science and Technology. We thank DOE/NETL Project Manager, Andrew O'Palko, for his assistance and support. The authors thank Dr. Xuehong Gu at Nanjing Tech University for providing hollow fiber support.

■ REFERENCES

(1) Song, Y.; Ozdemir, E.; Ramesh, S.; Adishev, A.; Subramanian, S.; Harale, A.; Albuali, M.; Fadhel, B. A.; Jamal, A.; Moon, D. Dry reforming of methane by stable Ni-Mo nanocatalysts on single-crystalline MgO. *Science* **2020**, *367* (6479), 777−781.

(2) De, S.; Zhang, J.; Luque, R.; Yan, N. Ni-based bimetallic heterogeneous catalysts for energy and environmental applications. *Energy Environ. Sci.* **2016**, *9* (11), 3314−3347.

(3) Field, C. B.; Mach, K. J. Rightsizing carbon dioxide removal. *Science* **2017**, *356* (6339), 706−707.

(4) Rockström, J.; Gaffney, O.; Rogelj, J.; Meinshausen, M.; Nakicenovic, N.; Schellnhuber, H. J. A roadmap for rapid decarbonization. *Science* **2017**, *355* (6331), 1269−1271.

(5) Pakhare, D.; Spivey, J. A review of dry (CO_2) reforming of methane over noble metal catalysts. *Chem. Soc. Rev.* **2014**, *43* (22), 7813−7837.

(6) Goula, M. A.; Charisiou, N. D.; Papageridis, K. N.; Delimitis, A.; Pachatouridou, E.; Iliopoulou, E. F. Nickel on alumina catalysts for the production of hydrogen rich mixtures via the biogas dry reforming reaction: Influence of the synthesis method. *Int. J. Hydrogen Energy* **2015**, *40* (30), 9183−9200.

(7) Charisiou, N.; Siakavelas, G.; Papageridis, K.; Baklavaridis, A.; Tzounis, L.; Avraam, D.; Goula, M. Syngas production via the biogas dry reforming reaction over nickel supported on modified with CeO_2 and/or La_2O_3 alumina catalysts. *J. Nat. Gas Sci. Eng.* **2016**, *31*, 164−183.

(8) Charisiou, N.; Siakavelas, G.; Tzounis, L.; Sebastian, V.; Monzon, A.; Baker, M.; Hinder, S.; Polychronopoulou, K.; Yentekakis, I.; Goula, M. An in depth investigation of deactivation through carbon formation during the biogas dry reforming reaction for Ni supported on modified with CeO_2 and La_2O_3 zirconia catalysts. *Int. J. Hydrogen Energy* **2018**, *43* (41), 18955−18976.

(9) Wernicke, H.-J.; Plass, L.; Schmidt, F. Methanol generation. In *Methanol: The basic chemical and energy feedstock of the future*; Springer: 2014; pp 51−301, DOI: 10.1007/978-3-642-39709-7_4.

(10) Zhong, L.; Yu, F.; An, Y.; Zhao, Y.; Sun, Y.; Li, Z.; Lin, T.; Lin, Y.; Qi, X.; Dai, Y. Cobalt carbide nanoprisms for direct production of lower olefins from syngas. *Nature* **2016**, *538* (7623), 84−87.

(11) Tristantini, D.; Lögdberg, S.; Gevert, B.; Borg, Ø.; Holmen, A. The effect of synthesis gas composition on the Fischer−Tropsch synthesis over Co/γ-Al_2O_3 and Co-Re/γ-Al_2O_3 catalysts. *Fuel Process. Technol.* **2007**, *88* (7), 643−649.

(12) Shi, L.; Yang, G.; Tao, K.; Yoneyama, Y.; Tan, Y.; Tsubaki, N. An introduction of CO_2 conversion by dry reforming with methane and new route of low-temperature methanol synthesis. *Acc. Chem. Res.* **2013**, *46* (8), 1838−1847.

(13) Gao, P.; Li, S.; Bu, X.; Dang, S.; Liu, Z.; Wang, H.; Zhong, L.; Qiu, M.; Yang, C.; Cai, J. Direct conversion of CO_2 into liquid fuels with high selectivity over a bifunctional catalyst. *Nat. Chem.* **2017**, *9* (10), 1019−1024.

(14) Jin, B.; Shang, Z.; Li, S.; Jiang, Y.-B.; Gu, X.; Liang, X. Reforming of methane with carbon dioxide over cerium oxide promoted nickel nanoparticles deposited on 4-channel hollow fibers by atomic layer deposition. *Catal. Sci. Technol.* **2020**, *10*, 3212−3222.

(15) Qin, Z.; Ren, J.; Miao, M.; Li, Z.; Lin, J.; Xie, K. The catalytic methanation of coke oven gas over Ni-Ce/Al_2O_3 catalysts prepared by microwave heating: Effect of amorphous NiO formation. *Appl. Catal., B* **2015**, *164*, 18−30.

(16) Akbari, E.; Alavi, S. M.; Rezaei, M. Synthesis gas production over highly active and stable nanostructured $NiMgOAl_2O_3$ catalysts in dry reforming of methane: Effects of Ni contents. *Fuel* **2017**, *194*, 171−179.

(17) Jin, B.; Li, S.; Liang, X. Enhanced activity and stability of MgO-promoted Ni/Al_2O_3 catalyst for dry reforming of methane: Role of MgO. *Fuel* **2021**, *284*, 119082.

(18) Li, K.; Pei, C.; Li, X.; Chen, S.; Zhang, X.; Liu, R.; Gong, J. Dry reforming of methane over $La_2O_2CO_3$-modified Ni/Al_2O_3 catalysts with moderate metal support interaction. *Appl. Catal., B* **2020**, *264*, 118448.

(19) Wei, J.; Iglesia, E. Isotopic and kinetic assessment of the mechanism of reactions of CH_4 with CO_2 or H_2O to form synthesis gas and carbon on nickel catalysts. *J. Catal.* **2004**, *224* (2), 370−383.

(20) Afandizadeh, S.; Foumeny, E. Design of packed bed reactors: Guides to catalyst shape, size, and loading selection. *Appl. Therm. Eng.* **2001**, *21* (6), 669−682.

(21) Liu, X.; Qin, B.; Zhang, Q.; Ye, G.; Zhou, X.; Yuan, W. Optimizing catalyst supports at single catalyst pellet and packed bed reactor levels: A comparison study. *AIChE. J.* **2021**, *67*, e17163.

(22) Yu, L.; Song, M.; Williams, P. T.; Wei, Y. Alumina-supported spinel $NiAl_2O_4$ as a catalyst for Re-forming pyrolysis gas. *Ind. Eng. Chem. Res.* **2019**, *58* (27), 11770−11778.

(23) Marinho, A. L.; Toniolo, F. S.; Noronha, F. B.; Epron, F.; Duprez, D.; Bion, N. Highly active and stable Ni dispersed on mesoporous CeO_2-Al_2O_3 catalysts for production of syngas by dry reforming of methane. *Appl. Catal., B* **2021**, *281*, 119459.

(24) Al-Megeren, H.; Xiao, T. Natural gas dual reforming catalyst and process. In *Advances in Natural Gas Technology*; InTech: 2012; pp 387−406, DOI: 10.5772/36790.

(25) Shi, Z.; Zhang, Y.; Cai, C.; Zhang, C.; Gu, X. Preparation and characterization of α-Al_2O_3 hollow fiber membranes with four-channel configuration. *Ceram. Int.* **2015**, *41* (1), 1333−1339.

(26) Kim, J.-H.; Suh, D. J.; Park, T.-J.; Kim, K.-L. Effect of metal particle size on coking during CO_2 reforming of CH_4 over Ni-alumina aerogel catalysts. *Appl. Catal., A* **2000**, *197* (2), 191−200.

(27) Liu, K.-I.; Kei, C.-C.; Mishra, M.; Chen, P.-H.; Liu, W.-S.; Perng, T.-P. Uniform coating of TiO_2 on high aspect ratio substrates with complex morphology by vertical forced-flow atomic layer deposition. *RSC Adv.* **2017**, *7* (55), 34730−34735.

(28) Li, F.; Yang, Y.; Fan, Y.; Xing, W.; Wang, Y. Modification of ceramic membranes for pore structure tailoring: The atomic layer deposition route. *J. Membr. Sci.* **2012**, *397*, 17−23.

(29) Jia, X.; Low, Z.; Chen, H.; Xiong, S.; Wang, Y. Atomic layer deposition of Al_2O_3 on porous polypropylene hollow fibers for enhanced membrane performances. *Chin. J. Chem. Eng.* **2018**, *26* (4), 695−700.

(30) Browne, M. P.; Plutnar, J.; Pourrahimi, A. M.; Sofer, Z.; Pumera, M. Atomic layer deposition as a general method turns any 3D-printed electrode into a desired catalyst: Case study in photoelectrochemisty. *Adv. Energy Mater.* **2019**, *9* (26), 1900994.

(31) Shang, Z.; Li, S.; Wang, Q.; Gu, X.; Liang, X. Nano-engineered nickel catalysts supported on 4-channel α-Al_2O_3 hollow fibers for dry reforming of methane. *AIChE J.* **2018**, *64* (7), 2625−2631.

(32) Scheffe, J. R.; Francés, A.; King, D. M.; Liang, X.; Branch, B. A.; Cavanagh, A. S.; George, S. M.; Weimer, A. W. Atomic layer deposition of iron (III) oxide on zirconia nanoparticles in a fluidized bed reactor using ferrocene and oxygen. *Thin Solid Films* **2009**, *517* (6), 1874−1879.

(33) Kessels, W.; Knoops, H.; Dielissen, S.; Mackus, A.; Van de Sanden, M. Surface reactions during atomic layer deposition of Pt derived from gas phase infrared spectroscopy. *Appl. Phys. Lett.* **2009**, *95* (1), 013114.

(34) Shang, Z.; Li, S.; Li, L.; Liu, G.; Liang, X. Highly active and stable alumina supported nickel nanoparticle catalysts for dry reforming of methane. *Appl. Catal., B* **2017**, *201*, 302−309.

(35) Rahemi, N.; Haghighi, M.; Babaluo, A. A.; Jafari, M. F.; Estifaee, P. Synthesis and physicochemical characterizations of Ni/Al_2O_3-ZrO_2 nanocatalyst prepared via impregnation method and treated with non-thermal plasma for CO_2 reforming of CH_4. *J. Ind. Eng. Chem.* **2013**, *19* (5), 1566−1576.
(36) Moradi, G.; Khezeli, F.; Hemmati, H. Syngas production with dry reforming of methane over Ni/ZSM-5 catalysts. *J. Nat. Gas Sci. Eng.* **2016**, *33*, 657−665.
(37) Roh, H.-S.; Potdar, H.; Jun, K.-W.; Kim, J.-W.; Oh, Y.-S. Carbon dioxide reforming of methane over Ni incorporated into Ce-ZrO_2 catalysts. *Appl. Catal., A* **2004**, *276* (1−2), 231−239.
(38) Huang, J.; Ma, R.; Huang, T.; Zhang, A.; Huang, W. Carbon dioxide reforming of methane over Ni/Mo/SBA-15-La_2O_3 catalyst: Its characterization and catalytic performance. *J. Nat. Gas Chem.* **2011**, *20* (5), 465−470.
(39) Wang, N.; Yu, X.; Shen, K.; Chu, W.; Qian, W. Synthesis, characterization and catalytic performance of MgO-coated Ni/SBA-15 catalysts for methane dry reforming to syngas and hydrogen. *Int. J. Hydrogen Energy* **2013**, *38* (23), 9718−9731.
(40) Fang, X.; Zhang, J.; Liu, J.; Wang, C.; Huang, Q.; Xu, X.; Peng, H.; Liu, W.; Wang, X.; Zhou, W. Methane dry reforming over Ni/Mg-Al-O: on the significant promotional effects of rare earth Ce and Nd metal oxides. *J. CO_2 Util.* **2018**, *25*, 242−253.
(41) Liu, D.; Quek, X. Y.; Cheo, W. N. E.; Lau, R.; Borgna, A.; Yang, Y. MCM-41 supported nickel-based bimetallic catalysts with superior stability during carbon dioxide reforming of methane: Effect of strong metal-support interaction. *J. Catal.* **2009**, *266* (2), 380−390.
(42) Chen, Q.; Zhang, J.; Pan, B.; Kong, W.; Chen, Y.; Zhang, W.; Sun, Y. Temperature-dependent anti-coking behaviors of highly stable Ni-CaO-ZrO_2 nanocomposite catalysts for CO_2 reforming of methane. *Chem. Eng. J.* **2017**, *320*, 63−73.
(43) Song, Z.; Wang, Q.; Guo, C.; Li, S.; Yan, W.; Jiao, W.; Qiu, L.; Yan, X.; Li, R. Improved effect of Fe on the stable NiFe/Al_2O_3 catalyst in low-temperature dry reforming of methane. *Ind. Eng. Chem. Res.* **2020**, *59* (39), 17250−17258.
(44) Zhang, G.; Wang, Y.; Li, X.; Bai, Y.; Zheng, L.; Wu, L.; Han, X. Effect of Gd promoter on the structure and catalytic performance of mesoporous Ni/Al_2O_3-CeO_2 in dry reforming of methane. *Ind. Eng. Chem. Res.* **2018**, *57* (50), 17076−17085.
(45) Luisetto, I.; Tuti, S.; Battocchio, C.; Mastro, S. L.; Sodo, A. Ni/CeO_2-Al_2O_3 catalysts for the dry reforming of methane: The effect of $CeAlO_3$ content and nickel crystallite size on catalytic activity and coke resistance. *Appl. Catal., A* **2015**, *500*, 12−22.
(46) Pantaleo, G.; La Parola, V.; Deganello, F.; Singha, R.; Bal, R.; Venezia, A. Ni/CeO_2 catalysts for methane partial oxidation: Synthesis driven structural and catalytic effects. *Appl. Catal., B* **2016**, *189*, 233−241.
(47) Ye, R.-P.; Li, Q.; Gong, W.; Wang, T.; Razink, J. J.; Lin, L.; Qin, Y.-Y.; Zhou, Z.; Adidharma, H.; Tang, J. High-performance of nanostructured Ni/CeO_2 catalyst on CO_2 methanation. *Appl. Catal., B* **2020**, *268*, 118474.
(48) Chen, W.; Zhao, G.; Xue, Q.; Chen, L.; Lu, Y. High carbon-resistance Ni/$CeAlO_3$-Al_2O_3 catalyst for CH_4/CO_2 reforming. *Appl. Catal., B* **2013**, *136*, 260−268.
(49) Damyanova, S.; Perez, C.; Schmal, M.; Bueno, J. M. Characterization of ceria-coated alumina carrier. *Appl. Catal., A* **2002**, *234* (1−2), 271−282.
(50) Kamonsuangkasem, K.; Therdthianwong, S.; Therdthianwong, A.; Thammajak, N. Remarkable activity and stability of Ni catalyst supported on CeO_2-Al_2O_3 via $CeAlO_3$ perovskite towards glycerol steam reforming for hydrogen production. *Appl. Catal., B* **2017**, *218*, 650−663.
(51) Pereira-Hernández, X. I.; DeLaRiva, A.; Muravev, V.; Kunwar, D.; Xiong, H.; Sudduth, B.; Engelhard, M.; Kovarik, L.; Hensen, E. J.; Wang, Y. Tuning Pt-CeO_2 interactions by high-temperature vapor-phase synthesis for improved reducibility of lattice oxygen. *Nat. Commun.* **2019**, *10* (1), 1358.
(52) Tang, Y.; Wei, Y.; Wang, Z.; Zhang, S.; Li, Y.; Nguyen, L.; Li, Y.; Zhou, Y.; Shen, W.; Tao, F. F. Synergy of single-atom Ni_1 and Ru_1 sites on CeO_2 for dry reforming of CH_4. *J. Am. Chem. Soc.* **2019**, *141* (18), 7283−7293.

https://doi.org/10.1021/acs.iecr.1c03705
Ind. Eng. Chem. Res. 2022, 61, 10377−10386